Journal of Southeast University (English Edition) Vol. 34, No. 3, pp. 364 - 370 Sept. 2018 ISSN 1003—7985

Damage evolution analysis of cast steel GS-20Mn5V based on modified GTN model

Yan Huadong Jin Hui

(Jiangsu Key Laboratory of Engineering Mechanics, Southeast University, Nanjing 211189, China)
(School of Civil Engineering, Southeast University, Nanjing 211189, China)

Abstract: A modified Gurson-Tvergaard-Needleman (GTN) model that accounts for the mixed (isotropic and kinematic) hardening of cast steel GS-20Mn5V was developed and implemented in the finite element program ABAQUS/Standard via a user-defined material subroutine UMAT. This model couples the stress state and damage evolution (pore volume fraction increase) by a classic method that assumes that the total void volume fraction is divided into a nucleation and a growth part. A parametric study was conducted to assess the effect of modified GTN model parameters on mechanical properties such as the nucleation, growth and coalescence of voids and to obtain the optimal parameter combination by the orthogonal test method. The predicted load-displacement curves of notched specimens with the optimal parameters are favorably compared to the experimental curves. Therefore, the modified GTN model can be used to predict the damage evaluation and fracture behavior of GS-20Mn5V.

Key words: cast steel; Gurson-Tvergaard-Needleman (GTN) model; damage evolution; orthogonal test method; optimal parameter combination

DOI: 10.3969/j.issn.1003-7985.2018.03.012

Cast steel is an important metal material that is widely used in civil engineering applications due to its strength and ductility[1]. Unfortunately, a variety of casting defects such as porosity and cracks are usually present in the as-cast components and can lead to the degradation of mechanical properties[2]. It is difficult to eliminate the porosity by modifying the casting technology due to cost impediments. Studies have demonstrated that both micro and macroporosity will affect the mechanical properties and fatigue life of castings[3]. When a casting is completed, the workers perform a nondestructive evaluation method (NDE), such as ultrasonic testing, to find the macroporosity and repair it. However, the resolution of NDE is insufficient to determine the size and location of the microporosity. To eliminate the influence of microporosity, designers employ excessively high safety factors to ensure reliability, leading to components that are heavier than necessary[4]. Therefore, understanding the effects of porosity on the mechanical properties of the cast steel is the key to assessing final life.

In recent decades, many scholars have explored the failure mode that results from the damage evolution mechanism of microporosity[5-8]. From a physical point of view, the damage of metallic materials can be divided into three stages: void nucleation, growth and coalescence[9]. Gurson[5] proposed an approximate yield function for a finite cell model with microvoids based on the work of Rice[10]. Then, Tvergaard[6-7] considered the interaction between voids and introduced three correction parameters to make the numerical results more consistent with the experimental results. Tvergaard and Needleman[8-9] introduced a damage function f^* to consider the effect of void coalescence. Therefore, the GTN damage model, which is one of the most widely used ductile damage models, was chosen to describe the fracture of metallic materials[10-12].

1 Modified GTN Constitutive Model

1.1 GTN constitutive model

The yield condition of the GTN model takes the following form[5-9]:

$$\varphi = \left(\frac{\sigma_{eq}}{\sigma_y}\right)^2 + 2q_1 f^* \cosh\left(-\frac{3q_2\sigma_m}{2\sigma_y}\right) - 1 + q_3 (f^*)^2 \quad (1)$$

where σ_y is the initial yield stress of the matrix material; σ_{eq} is the effective Von Mises stress; σ_m is the hydrostatic stress; three arbitrary parameters q_1, q_2 and q_3 are introduced by Tvergaard[6-7] to make the prediction of the Gurson equation agree with numerical results; f is the actual void volume fraction. The effective porosity volume fraction f^* is introduced by Tvergaard et al.[8-9] to account for the final material failure for void coalescence, which is a function of the actual void volume fraction f and is expressed as

Received 2017-11-12, **Revised** 2018-03-17.

Biographies: Yan Huadong (1990—), female, Ph. D. candidate; Jin Hui (corresponding author), female, doctor, professor, jinhui@seu.edu.cn.

Foundation items: The National Key Research and Development Program of China (No. 2017YFC0805103). the National Natural Science Foundation of China (No. 51578137, 51438002, 51108075), the Open Research Fund Program of Jiangsu Key Laboratory of Engineering Mechanics.

Citation: Yan Huadong, Jin Hui. Damage evolution analysis of cast steel GS-20Mn5V based on modified GTN model[J]. Journal of Southeast University (English Edition), 2018, 34(3): 364 - 370. DOI: 10.3969/j.issn.1003-7985.2018.03.012.

$$f^*(f)=\begin{cases} f & f\leqslant f_c \\ f_c+\dfrac{f_u^*-f_c}{f_F-f_c}(f-f_c) & f_c<f\leqslant f_F \\ f_u^* & f>f_F \end{cases} \quad (2)$$

where f_c is the critical void volume fraction of void coalescence and f_F is the final void volume fraction when the material fails. When the material has completely lost its stress carrying capacity, f_u^* is defined as

$$f_u^*=1/q_1 \quad (3)$$

According to Ref. [8], the growth rate of the actual void volume fraction f is defined as the sum of the growth of existing voids and the nucleation of new voids:

$$\mathrm{d}f=\mathrm{d}f_{\text{growth}}+\mathrm{d}f_{\text{nucleation}} \quad (4)$$

The rate of void growth $\mathrm{d}f_{\text{growth}}$ is proportional to the actual void volume fraction f and the plastic strain rate $\mathrm{d}\varepsilon_{ij}^{\mathrm{p}}$:

$$\mathrm{d}f_{\text{growth}}=(1-f)\,\mathrm{d}\varepsilon_{ij}^{\mathrm{p}} \quad (5)$$

In the nucleation term, the equivalent plastic strain rate $\mathrm{d}\varepsilon^{\mathrm{pl}}$ is the exclusive dependent variable:

$$\mathrm{d}f_{\text{nucleation}}=A\mathrm{d}\varepsilon^{\mathrm{pl}} \quad (6)$$

The void nucleation intensity A is a function[13] of the volume fraction of all particles with potential for microvoid nucleation f_N, the mean nucleation strain ε_N and the corresponding standard deviation S_N.

$$A=\frac{f_N}{S_N\sqrt{2\pi}}\exp\left[-\frac{1}{2}\left(\frac{\mathrm{d}\varepsilon^{\mathrm{pl}}-\varepsilon_N}{S_N}\right)^2\right] \quad (7)$$

In a metallic material, the plastic flow depends on the actual void volume fraction f and the equivalent plastic strain $\varepsilon^{\mathrm{pl}}$. According to the equivalent work principle, the evolution equation of equivalent plastic strain is given by[14]

$$\mathrm{d}\varepsilon^{\mathrm{pl}}=\frac{\sigma_{ij}\mathrm{d}\varepsilon_{ij}^{\mathrm{p}}}{(1-f)\sigma_m} \quad (8)$$

1.2 The mixed hardening model

The yield surface is usually a constant of the ideal elastoplastic materials. However, the plastic deformation of the practical materials shows a more pronounced hardening effect, and the yield surface will change with the development of plastic deformation. There are three hardening models: the isotropic hardening model, the kinematic hardening model and the mixed hardening model.

The isotropic hardening model assumes that the yield surface expands uniformly under loading, while the yield surface center moves parallel to the hardening curve in the kinematic hardening model. In fact, many practical materials show a combined effect of isotropic and kinematic hardening behavior. To address this case, a mixed hardening model is introduced to address the change in the yield stress and the back stress[15-16].

The general formulation of a mixed hardening model is as follows:

$$\varphi(\sigma_{ij}-\alpha_{ij})-k(\kappa)=0 \quad (9)$$

where σ_{ij} is the Cauchy stress tensor; the back stress tensor α_{ij} is used to describe the movement of the yield surface center in the stress space; and $k(\kappa)$ is used to describe the expansion of the yield surface with the increasing plastic strain.

Yield stress σ is the a function of equivalent plastic strain $\varepsilon^{\mathrm{pl}}$, and σ defines the evolution of the yield surface. Yield stress is expressed as an exponential equation[15]:

$$\sigma=\sigma_y+a[1-\exp(-b\varepsilon^{\mathrm{pl}})] \quad (10)$$

where a and b are the hardening coefficient and exponent, respectively, which can be fitted by the true stress-plastic strain curve.

Frederick and Armstrong[16] proposed a kinematic hardening model which can calculate the change in back stress,

$$\mathrm{d}\alpha_{ij}=\frac{2}{3}C\mathrm{d}\varepsilon_{ij}^{\mathrm{p}}-\gamma\alpha_{ij}\mathrm{d}\varepsilon^{\mathrm{pl}} \quad (11)$$

where C and γ are material constants.

When the material is subjected to auniaxial tensile load, Eq. (11) can be expressed as

$$\alpha_1=\frac{2}{3}\frac{C}{\gamma}[1-\exp(-\gamma\varepsilon_1^{\mathrm{p}})] \quad (12)$$

In contrast to Eqs. (10) and (12), C and γ can be obtained using the following equation:

$$C=\frac{3}{2}\gamma a \quad (13)$$

$$\gamma=b \quad (14)$$

1.3 A modified GTN model accounting for the mixed hardening

To apply the research results to practical engineering analysis, the modified GTN constitutive relationship considers the influence of back stress and yield surface expansion on the basis of the classical GTN damage theory. Σ_{ij} is the difference between Cauchy stress σ_{ij} and back stress α_{ij}:

$$\Sigma_{ij}=\sigma_{ij}-\alpha_{ij} \quad (15)$$

The effective Von Mises stress and the hydrostatic stress can be expressed as

$$Q=\sqrt{\frac{3}{2}\Sigma'_{ij}\Sigma'_{ij}} \quad (16)$$

$$P = -\frac{1}{3}\Sigma_{mm} \tag{17}$$

where Σ'_{ij} and Σ_{mm} are the deviatoric stress and the hydrostatic stress of Σ_{ij}, respectively.

The yield function of the modified GTN model is given by

$$\Phi = \left(\frac{Q}{\sigma}\right)^2 + 2q_1 f^* \cosh\left(-\frac{3q_2 P}{2\sigma}\right) - 1 + q_3 (f^*)^2 \tag{18}$$

According to the classical numerical integration of the elastoplastic constitutive relationships[14, 17], the modified GTN model can be implemented in the finite element program ABAQUS/Standard via a user-defined material subroutine UMAT.

2 Finite Element Analysis

2.1 Material mechanical testing

The material used in this study is cast steel GS-20Mn5V. It is a cast carbon steel that has both good ductility and high strength. It has the following chemical composition: C 0.17 to 0.23; Si 0.6; Mn 1.00 to 1.50; P 0.025; S 0.020; Cr 0.30; Mo 0.15; Ni 0.40. The objective of the experimental program in Ref. [18] studied the mechanical properties of cast steel GS-20Mn5V under uniaxial tensile stresses.

The dimensions of the tensile specimens (smooth and notched) are shown in Fig. 1. The basic mechanical properties of GS-20Mn5V are listed in Tab. 1. The load-displacement curves of the specimens with a 1 mm or 4 mm notch radius are discrete, while the load-displacement curves of the specimens with a 2 mm notch radius are in good agreement. Therefore, the experimental data of the ZR2-1 specimen are chosen to compare with the numerical simulation in Section 2. In Fig. 2, the point with an abrupt change in the slope in the descent section of the load-displacement curve indicates specimen fracture[18-19]. The purpose of this paper is to predict the location of the fracture point using a modified GTN model to demonstrate its ability to predict crack growth in cast steel GS-20Mn5V.

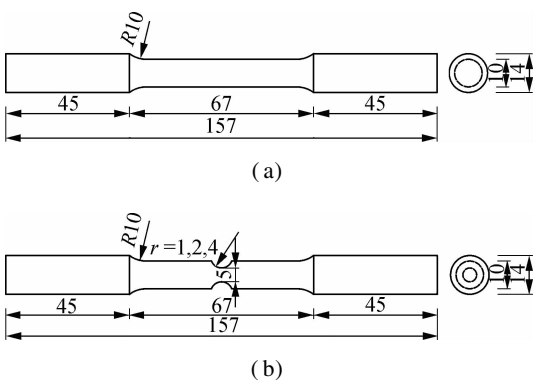

Fig. 1 Geometry and dimensions of the specimens used in the tensile test (unit: mm). (a) Smooth specimen; (b) Notched specimen

Tab. 1 Mechanical properties of cast steel GS-20Mn5V

E/GPa	v	σ_y^0/MPa	σ_u/MPa	a/MPa	b
209	0.3	290	612	382.41	10.79

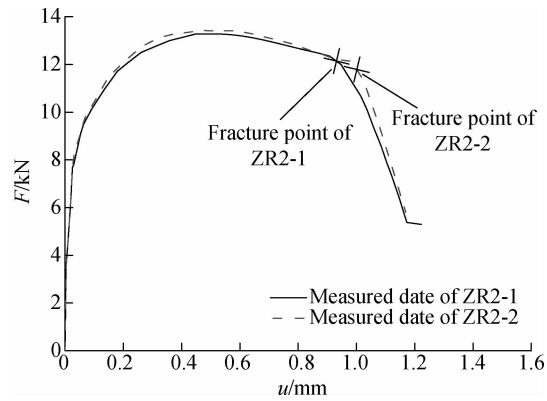

Fig. 2 Load-displacement curves for notched specimens with r = 2 mm

2.2 Mesh sensitivity analysis of the finite element model

A one-quarter-scale finite element model of the notched specimen (notch radius r = 2 mm) was established in ABAQUS, and an axial displacement load was applied (see Fig. 3). To analyze the dependence of the simulation results on the computational mesh density, six different nodal mesh spacings of 2, 1.5, 1, 0.5, 0.3 and 0.1 mm are used to segment the notched part of the finite element model. The same material parameters are used for the finite element models with different mesh densities, and the specific values can be found in Tab. 1 and Tab. 2[18].

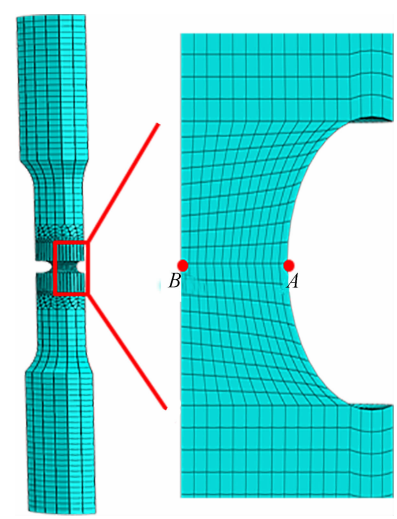

Fig. 3 The finite element model for the notched specimen

Tab. 2 Model parameters for the mesh sensitivity analysis

q_1	q_2	q_3	f_0	f_c	f_N	f_F	ε_N	S_N
1.9	0.3	3.61	0.001	0.2	0.02	0.35	0.3	0.1

In Fig. 4, the effective porosity volume fraction f^* at Point B (located at the center of the notch, as shown in Fig. 3) is extracted to show the damage evolution process. When the mesh size is larger than 1 mm, the damage evolution curves at Point B change gradually. The 2 and 1.5 mm damage evolution curves are very similar, and the simulated damage evolution curves for the 0.3 and 0.1 mm mesh spacings appear to converge. Based on this grid convergence study, the 0.3 mm mesh spacing was used to simulate the notched specimens. The 0.1 mm mesh spacing had an overly long computation time when simulating all the specimens.

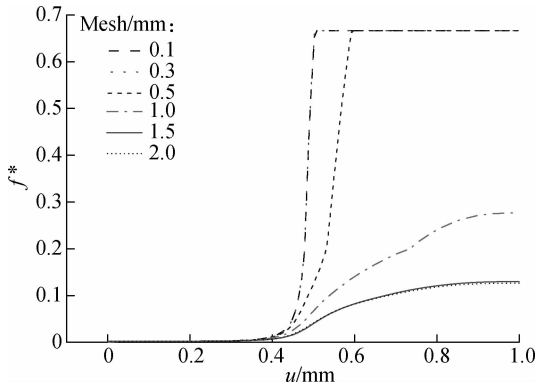

Fig. 4 The damage evolution curves obtained from grid dependence studies for a notched specimen at Point B

2.3 Determination of the modified GTN damage model parameters

The nine GTN parameters of cast steel GS-20Mn5V were determined by comparing the numerical simulation load-displacement curves with the measured curves. q_1, q_2 and q_3 are 1.5, 1.0, and 2.25, respectively, according to Tvergaard and Hutchinson[20]. Chu and Needleman[13] noted that the mean nucleation strain ε_N and the corresponding standard deviation S_N were 0.3 and 0.1, respectively, which are applicable to the majority of materials and have been widely recognized by researchers. Since the damage process and fracture mechanism of materials are highly complex, the void volume fractions f_0, f_N, f_c, and f_F were calibrated individually[12, 21].

2.3.1 Effect of f_0 on the mechanical properties

Zhang[18] summarized the GTN parameter reference for a variety of materials. The initial volume fraction f_0 is typically between 0.000 1 and 0.007. In this paper, three values 0.000 1, 0.002 and 0.005 are chosen to determine the influence of f_0 on the tensile properties. As shown in Fig. 5, the value of f_0 influences the maximum load of the load-displacement curves of notched specimens. Higher f_0 values allow the maximum load to increase while maintaining the same slope of the curves after the final fracture point, thus leaving the fracture position largely unchanged.

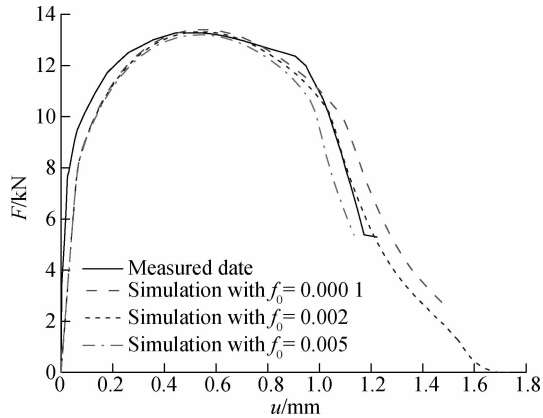

Fig. 5 Effect of varying f_0 on the predicted load-displacement curves compared to the measured curves

2.3.2 Effect of f_N on the mechanical properties

As shown in Fig. 6, the f_N value influences the elongation of notched specimens at the fracture point. A higher f_N can lead to a lower ductility of the specimen for a constant slope of the curves after fracture.

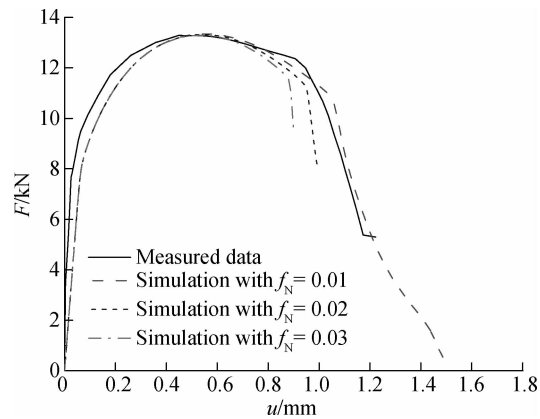

Fig. 6 Effect of varying f_N on the predicted load-displacement curves compared to the measured curves

2.3.3 Effect of f_c on the mechanical properties

As shown in Fig. 7, increasing the coalescence void volume fraction from 0.02 to 0.04 increases the fracture

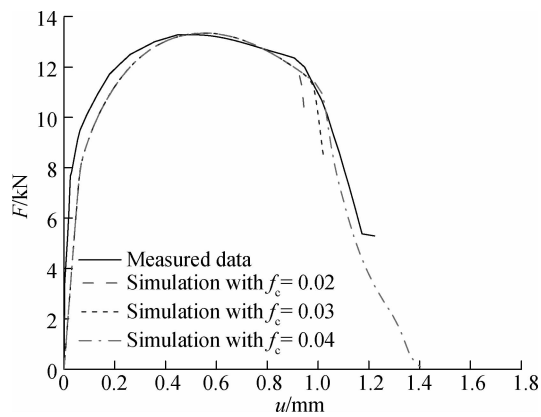

Fig. 7 Effect of f_c on the predicted load-displacement curves compared to the measured curves

position and the fracture ductility of the load-displacement curves of notched specimens, whereas the slopes of the curves after the fracture point are not affected by the f_c values.

2.3.4 Effect of f_F on the mechanical properties

The load-displacement curves with different values of f_F are shown in Fig. 8. f_F has only a slight effect on the failure position of the notched specimens, which is related to the slope after the failure of the material. A steeper slope can be obtained with a lower f_F value.

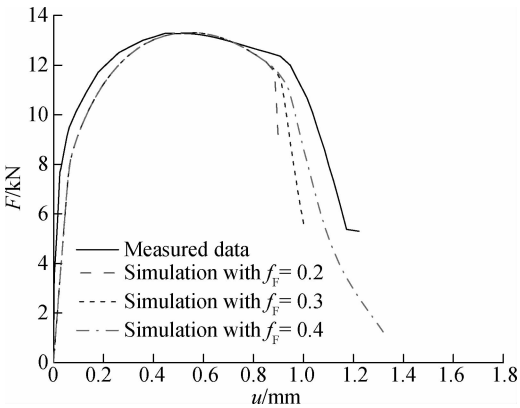

Fig. 8 Effect of f_F on the predicted load-displacement curves compared to the measured curves

2.4 Orthogonal test method

The orthogonal test method is a mathematical statistical method used to arrange and analyze a multifactor experiment with an orthogonal table[22]. The purpose of this method is to obtain the most representative combination of experimental factors with the highest efficiency.

The ranges in variation of the GTN model parameters for cast steel GS-20Mn5V, which are the factors of the array, are chosen according to Section 2.3. The porosity fractions are as follows: f_0 is 0.000 1 to 0.005; f_c is 0.02 to 0.04; f_F is 0.2 to 0.4; and f_N is 0.01 to 0.03. These four parameters are divided into three levels, as shown in Tab. 3, and an orthogonal test is carried out, using the orthogonal array $L_9(3^4)$, as shown in Tab. 4.

Tab. 3 Ranges of variation in the GTN parameters for GS-20Mn5V

Levels	f_0	f_c	f_F	f_N
1	0.002	0.02	0.4	0.01
2	0.005	0.03	0.3	0.02
3	0.000 1	0.04	0.2	0.03

According to the ductile fracture mechanism, f_c is greater than f_0 and f_N and less than f_F. Therefore, models 4, 7, and 8 should be abandoned. The load-displacement curves of the remaining 6 models were compared with the test results of the ZR2-1 notched specimen, and the results are shown in Fig. 9. Based on this figure, their preferred values can be obtained by orthogonal analysis, and the optimal parameter combination in the modified GTN model for cast steel GS-20Mn5V is shown in Tab. 5.

Tab. 4 $L_9(3^4)$ orthogonal array testing for the GTN model

Orthogonal model	f_0	f_c	f_F	f_N
1	0.002	0.02	0.4	0.01
2	0.002	0.03	0.3	0.02
3	0.002	0.04	0.2	0.03
4	0.005	0.02	0.3	0.03
5	0.005	0.03	0.2	0.01
6	0.005	0.04	0.4	0.02
7	0.000 1	0.02	0.2	0.02
8	0.000 1	0.03	0.4	0.03
9	0.000 1	0.04	0.3	0.01

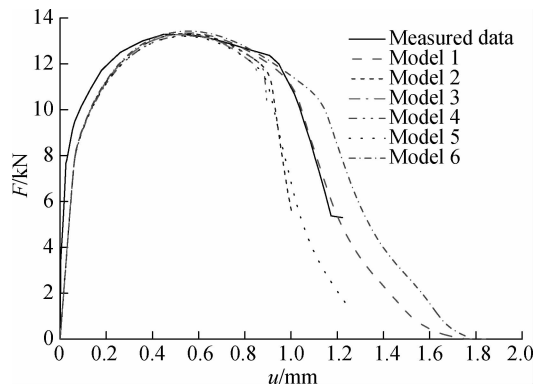

Fig. 9 Predicted load-displacement curves of the orthogonal test models

Tab. 5 Optimal parameter combination in the GTN model for the GS-20Mn5V cast steel

q_1	q_2	q_3	f_0	f_c	f_N	f_F	ε_N	S_N
1.5	1.0	2.25	0.002	0.02	0.01	0.4	0.3	0.1

3 Damage Evolution Prediction for GS-20Mn5V

The measured and simulated (with the GTN model in Ref. [18] and with the modified GTN model) load-displacement curves of the ZR2-1 notched specimen are shown in Fig. 10. The measured and predicted fracture positions for ZR2-1 are marked with a fork. By observing the locations of these three points, the predicted fracture position with the modified GTN model is closer to the actual fracture position, and, after the propagation, the slopes of the load-displacement curves also correspond well. Therefore, the modified GTN damage model with the optimal parameters accurately predicts reduction in ductility and fracture behavior. Three points along the predicted tensile curve are shown in Fig. 10 to demonstrate the relationship of the failure process and damage evolution. The testing displacements are approximately 0.6, 1.0, and 1.2 mm at Points 1, 2, and 3, respectively. Point 1 is at the position of the ultimate tensile strength; Point 2 is the measured breaking point, which indicates the fracture of the specimen; and Point 3 is located at the point of complete failure of the notched specimen.

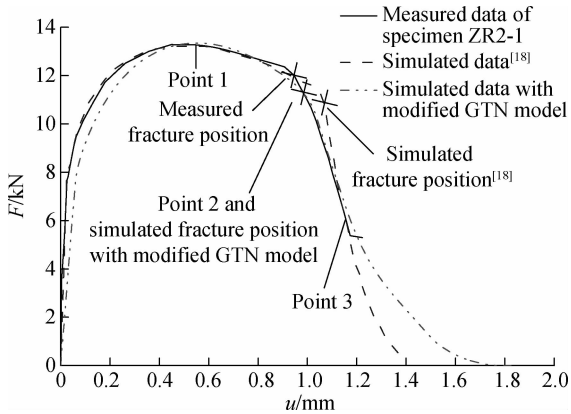

Fig. 10 Simulated and measured load-displacement curves for ZR2-1 notched specimen

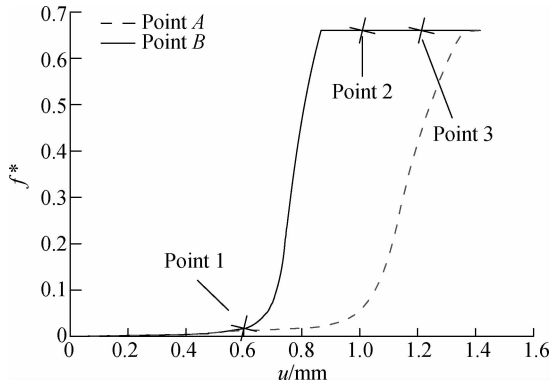

Fig. 11 Damage elevation curves of ZR2-1 notched specimens at Points *A* and *B*

The damage f^* evolution process of the notched specimens at Points *A* and *B* (see Fig. 3) is shown in Fig. 11. The extreme damage value is set to to be $1/q_1 = 0.666\,7$, i. e., the unit failure when the damage reaches the maximum value. In Fig. 11, the results of the damage fraction at Point 1 are lower than the critical void volume fraction for void coalescence f_c. Before Point 1, the damage evolution is slow. However, beyond this point, the load bearing capacity of the notched specimens decreases with the accelerated damage evolution. From Points 1 to 3, the damage value increases due to the nucleation and growth of voids until failure occurs.

The microscopic fracture process of the specimen in Fig. 12 shows the failure behavior of the notched specimens. Fig. 12(a) illustrates a crack initiated at the center of the notched specimen (Point *B*). With increasing displacement, the crack extends to the surface of the specimen (see Fig. 12(b)). Finally, the overall fracture nephogram is shown in Fig. 12(c). The simulation of the crack initiation and propagation process with the modified GTN model corresponds well with the actual fracture process of notched tensile specimens[19].

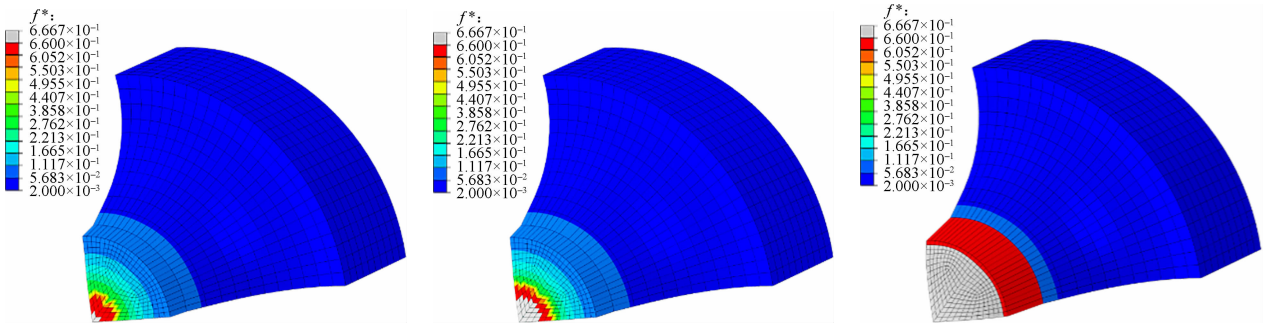

(a) (b) (c)

Fig. 12 Microscopic failure process of the notched specimen. (a) Crack initiation; (b) Crack propagation; (c) Fracture

4 Conclusion

A modified GTN model with mixed hardening was described to simulate the damage and fracture behaviors of notched tensile specimens. The effects of f_0, f_N, f_c, and f_F on the mechanical behavior of the specimen were investigated using numerical analysis, and the optimal parameter combination in the GTN model of cast steel GS-20Mn5V was obtained by an orthogonal test method. Based on these simulated results, the damage evolution process of steel castings can be predicted simply and accurately.

References

[1] Haldimann-Sturm S C, Nussbaumer A. Fatigue design of cast steel nodes in tubular bridge structures [J]. *International Journal of Fatigue*, 2008, **30**(3): 528 − 537. DOI: 10.1016/j.ijfatigue.2007.03.007.

[2] Wang Q G, Jones P E. Prediction of fatigue performance in aluminum shape castings containing defects [J]. *Metallurgical & Materials Transactions B*, 2007, **38**(4): 615 − 621. DOI: 10.1007/s11663-007-9051-4.

[3] Gao Y X, Yi J Z, Lee P D, et al. The effect of porosity on the fatigue life of cast aluminium-silicon alloys [J]. *Fatigue & Fracture of Engineering Materials & Structures*, 2004, **27**(7): 559 − 570. DOI: 10.1111/j.1460-2695.2004.00780.x.

[4] Sigl K M, Hardin R A, Stephens R I, et al. Fatigue of 8630 cast steel in the presence of porosity [J]. *International Journal of Cast Metals Research*, 2004, **17**(3): 130 − 146. DOI: 10.1179/136404604225020588.

[5] Gurson A L. Continuum theory of ductile rupture by void

nucleation and growth: Part I—Yield criteria and flow rules for porous ductile media [J]. *Journal of Engineering Materials and Technology*, 1977, **99**(1): 297 - 300. DOI: 10.1115/1.3443401.

[6] Tvergaard V. Influence of voids on shear band instabilities under plane strain conditions [J]. *International Journal of Fracture*, 1981, **17**(4): 389 - 407. DOI: 10.1007/bf00036191.

[7] Tvergaard V. On localization in ductile materials containing spherical voids [J]. *International Journal of Fracture*, 1982, **18**(4): 237 - 252. DOI: 10.1007/BF00015686.

[8] Tvergaard V, Needleman A. Analysis of the cup-cone fracture in a round tensile bar [J]. *Acta Metallurgica*, 1984, **32**(1): 157 - 169. DOI: 10.1016/0001-6160(84)90213-x.

[9] Needleman A, Tvergaard V. An analysis of ductile rupture in notched bars [J]. *Journal of the Mechanics and Physics of Solids*, 1984, **32**(6): 461 - 490. DOI: 10.1016/0022-5096(84)90031-0.

[10] Rice J R, Tracey D M. On the ductile enlargement of voids in triaxial stress fields[J]. *Journal of the Mechanics & Physics of Solids*, 1969, **17**(3): 201 - 217.

[11] Barrera O, Tarleton E, Tang H W, et al. Modelling the coupling between hydrogen diffusion and the mechanical behaviour of metals [J]. *Computational Materials Science*, 2016, **122**: 219 - 228. DOI: 10.1016/j.commatsci.2016.05.030.

[12] Tu H, Schmauder S, Weber U. Numerical study of electron beam welded butt joints with the GTN model [J]. *Computational Mechanics*, 2012, **50**(2): 245 - 255. DOI: 10.1007/s00466-012-0739-1.

[13] Chu C C, Needleman A. Void nucleation effects in biaxially stretched sheets [J]. *Journal of Engineering Materials & Technology*, 1980, **102**(3): 249. DOI: 10.1115/1.3224807.

[14] Aravas N. On the numerical integration of a class of pressure-dependent plasticity models [J]. *International Journal for Numerical Methods in Engineering*, 1987, **24**(7): 1395 - 1416. DOI: 10.1002/nme.1620240713.

[15] Lemaitre J. Aspect phenomenologique de la rupture par endommagement [J]. *Journal de Mecanique Appliquee*, 1978, **2**(3): 317 - 365.

[16] Frederick C O, Armstrong P J. A mathematical representation of the multiaxial Bauschinger effect [J]. *Materials at High Temperatures*, 2007, **24**(1): 1 - 26. DOI: 10.3184/096034007x207589.

[17] Zhang Z L. On the accuracies of numerical integration algorithms for Gurson-based pressure-dependent elastoplastic constitutive models [J]. *Computer Methods in Applied Mechanics and Engineering*, 1995, **121**(1): 15 - 28. DOI: 10.1016/0045-7825(94)00706-s.

[18] Zhang P. Study on fracture prediction of building steel joints using micro-mechanical GTN model [D]. Beijing: School of Civil Engineering, Beijing Jiaotong University, 2014. (in Chinese)

[19] Tong X W, Tong L W, Zhou F, et al. Fracture prediction of welded beam-to-column joints based on micromechanics damage model [J]. *Journal of Building Structures*, 2013, **34**(11): 82 - 90. (in Chinese)

[20] Tvergaard V, Hutchinson J W. The relation between crack growth resistance and fracture process parameters in elastic-plastic solids [J]. *Journal of the Mechanics and Physics of Solids*, 1992, **40**(6): 1377 - 1397. DOI: 10.1016/0022-5096(92)90020-3.

[21] Sun G Q, Sun F Y, Cao F L, et al. Numerical simulation of tension properties for Al-Cu alloy friction stir-welded joints with GTN damage model [J]. *Journal of Materials Engineering and Performance*, 2015, **24**(11): 4358 - 4363. DOI: 10.1007/s11665-015-1715-7.

[22] Kang L, Dixon S, Wang K, et al. Enhancement of signal amplitude of surface wave EMATs based on 3-D simulation analysis and orthogonal test method [J]. *Ndt & E International*, 2013, **59**: 11 - 17. DOI: 10.1016/j.ndteint.2013.05.003.

基于改进 GTN 模型铸钢 GS-20Mn5V 的损伤演化分析

闫华东　靳　慧

（东南大学江苏省工程力学分析重点实验室，南京 211189）
（东南大学土木工程学院，南京 211189）

摘要：改进的 Gurson-Tvergaard-Needleman（GTN）模型考虑了铸钢 GS-20Mn5V 的混合硬化（各向同性硬化和随动硬化）行为，并通过用户材料子程序 UMAT 将该模型嵌入商业有限元软件 ABAQUS/Standard 中. 改进的 GTN 模型将孔洞体积分数的增长假设为原有孔洞的长大和新孔洞的形核，并通过这一经典假设将材料的应力状态和损伤演化（孔洞体积分数增加）有效耦合. 详细研究了修正 GTN 模型中各参数对孔洞形核、生长和聚合等各阶段力学行为的影响，并通过正交试验方法得到了最优参数组合. 通过最优参数组合模拟得到的缺口试样载荷-位移曲线与试验测得的曲线对比，吻合度较高. 因此，可利用改进的 GTN 模型对 GS-20Mn5V 铸钢试件的损伤演化和断裂进行预测.

关键词：铸钢；GTN 模型；损伤演化；正交试验法；最优参数组合

中图分类号：TU512.9